Supplementary Information

A fluidic device for continuous on-line inductive sensing of proteolytic cleavages

*Fan Li,[‡1] Leif Sieben,[‡1,2] Johannes Büchler,[1] Manuel Strahm,[1,3] Pascal Poc,[1] Matej Vizovišek,[1] Michael G. Christiansen,[1 *] and Simone Schuerle[1 *]*

Affiliations

[1] Institute of Translational Medicine, Department of Health Sciences and Technology, ETH Zurich, 8092 Zurich, Switzerland

[2] Department of Chemistry and Applied Biosciences, ETH Zürich, 8093 Zürich, Switzerland

[3] Department of Information Technology and Electrical Engineering, ETH Zürich, 8092 Zürich, Switzerland.

[*] Authors to whom correspondence should be addressed: michael.christiansen@hest.ethz.ch and simone.schuerle@hest.ethz.ch

[‡] These authors contributed equally to this work.

Supplementary Methods

Cleavage efficiency of the peptide with different proteases. A fluorogenic peptide substrate, Dabcyl-VGFYESDVE(EDANS)-NH_2 (synthesized by Caslo ApS), was used to evaluate the cleavage efficiency. 100 µM substrate was incubated with different proteases at concentrations ranging from 0.05 to 3.2 nM in a reaction buffer (30 mM Tris HCl, 5 mM $CaCl_2$, pH 8.0) at 37°C. Protease conditions included specific proteases (chymotrypsin, TEV protease), a non-specific protease (proteinase K), and controls (pepsin, and no protease). Fluorescence intensity was measured over time (excitation at 360 nm, emission at 485 nm) using a microplate reader (TECAN Spark Multimode Microplate Reader). The cleavage product was calibrated against a standard curve of free EDANS (MedChem Express, HY-D1080R).

Cleavage site determination of the peptide with LC-MS analysis. 100 µM peptide DBCO-VGFYESDVC-NH_2 (1) was incubated with 1 µM protease at 37°C in a reaction buffer (30 mM Tris HCl, 5 mM $CaCl_2$, pH 8.0). After 5 min, 100 µL of the reaction mixture was quenched in 100 µL water/acetonitrile 1:1 containing 1 % formic acid. Each sample was analyzed by a LC-MS system (Agilent OpenLAB CDS 2.8). 10 µL sample were injected into an Agilent 1290 HPLC system equipped with a single quadrupole MSD over an Agilent Poroshell 120 SB-C18 column (1.9 µm 3 × 50 mm) heated at 40°C, using water/acetonitrile 95:5 and acetonitrile containing 0.2% formic acid as solvent A and B, respectively. The following LC method was used: 0–1 min, B= 0%; 1–4 min, B= 0−95%; 4-5 min, B= 95%.

Supplementary Figures

A) Detailed schematic of capacitive discharge circuit used to generate pulses

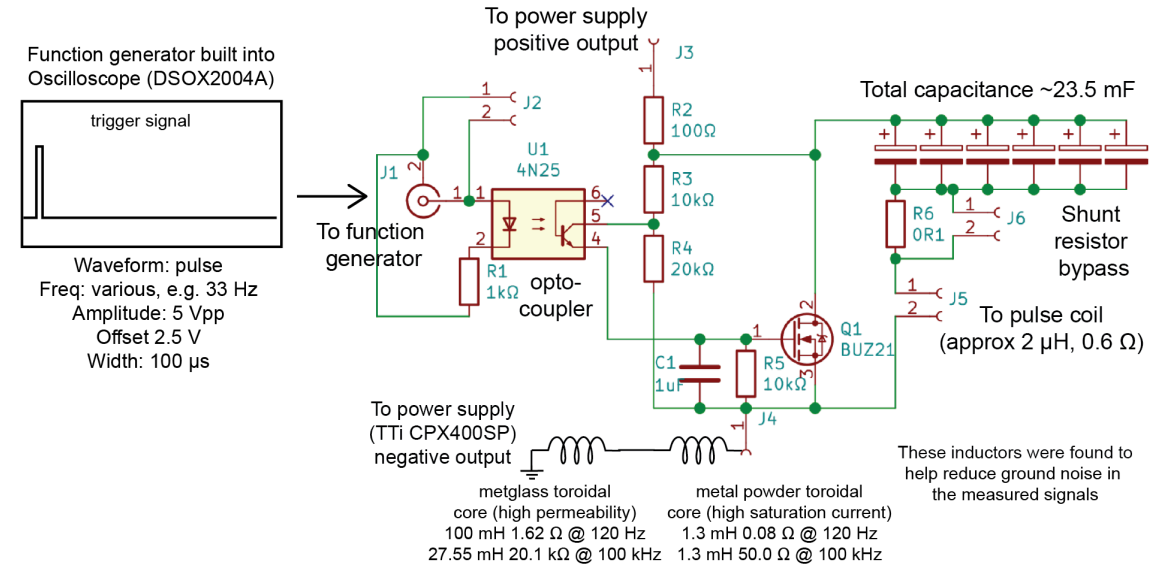

B) Photograph of printed circuit board

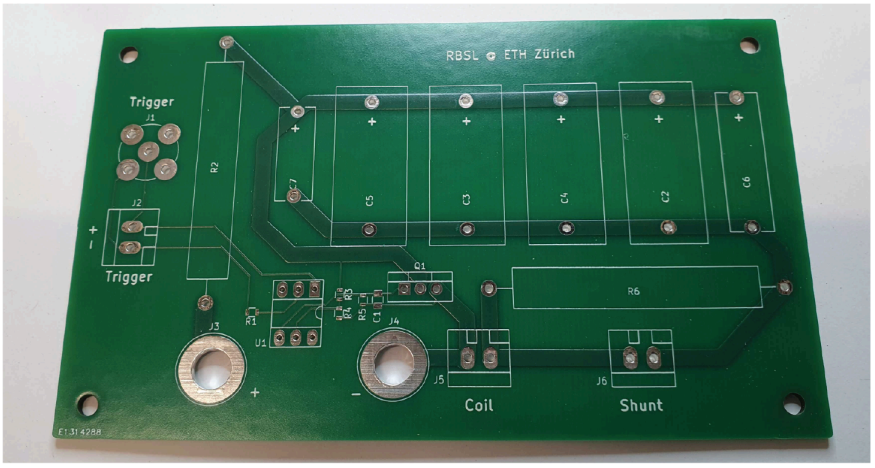

Supplementary Figure S1: Capacitive discharge circuit. A) A detailed schematic of the pulse circuit is shown, including information about equipment and components located off of the printed circuit board, such as the power supply that charges the capacitors and the inductors introduced to reduce ground noise. B) A photograph of the unpopulated printed circuit board for the pulse circuit is shown.

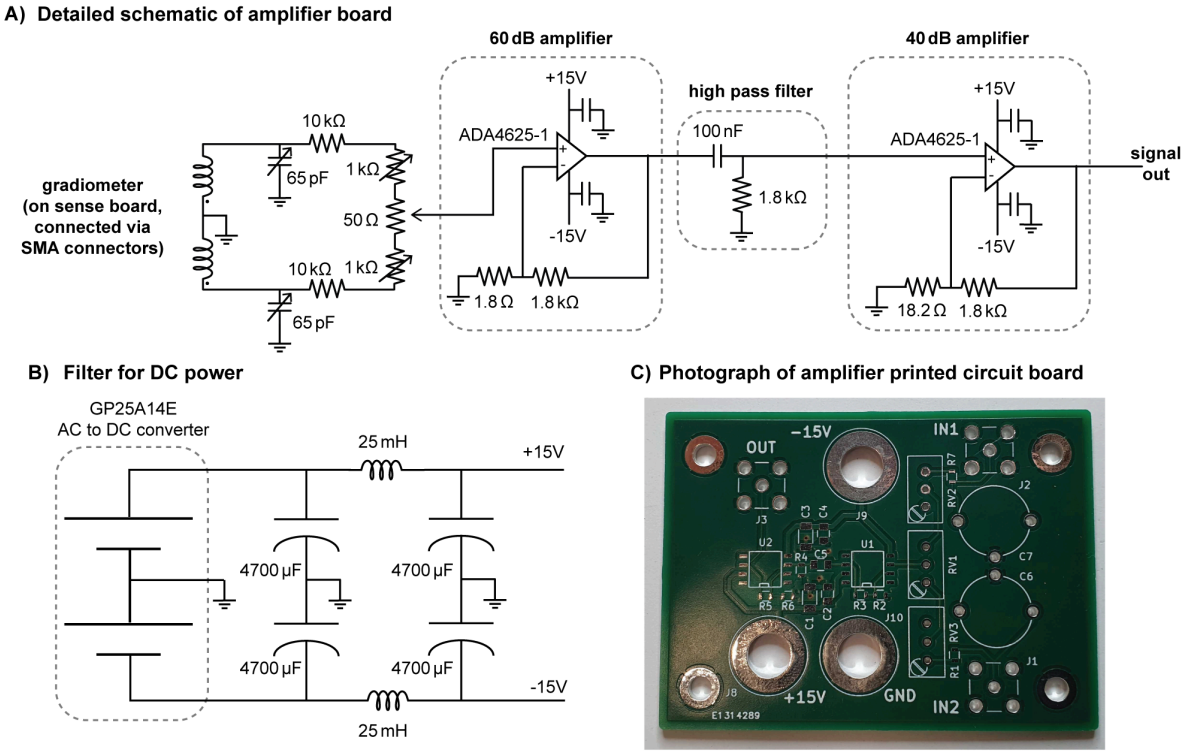

Supplementary Figure S2: Amplifier board. A) A detailed schematic of the amplifier board is shown, including values of the components actually used. For clarity, the gradiometer coils are shown, though in practice they are joined through two SMA connectors (IN1 and IN2). The parasitic capacitance and inductance of the SMA connections is neglected. Two 65 pF variable capacitors are provided nominally to adjust self resonance of the two gradiometer coils and ensure better cancellation. Three variable resistors are provided, two of which are 1 kΩ and provide a mechanism for coarse adjustment. The center one is 50 Ω, signal is taken from its wiper, and it provides fine adjustment of cancellation between the two coils. The amplification consists of two stages, separated by a high pass filter. The first provides a gain of 60 dB and the second provides a gain of 40 dB, giving an estimated overall amplification of 100 dB. B) A detailed schematic of the Pi-filter in series with the power supply is shown for the ±15V DC voltage applied to the boards. This filter was introduced to avoid the introduction of noise from the AC to DC converter into the recorded signals. C) A photograph of the unpopulated printed circuit board for the amplifiers is shown.

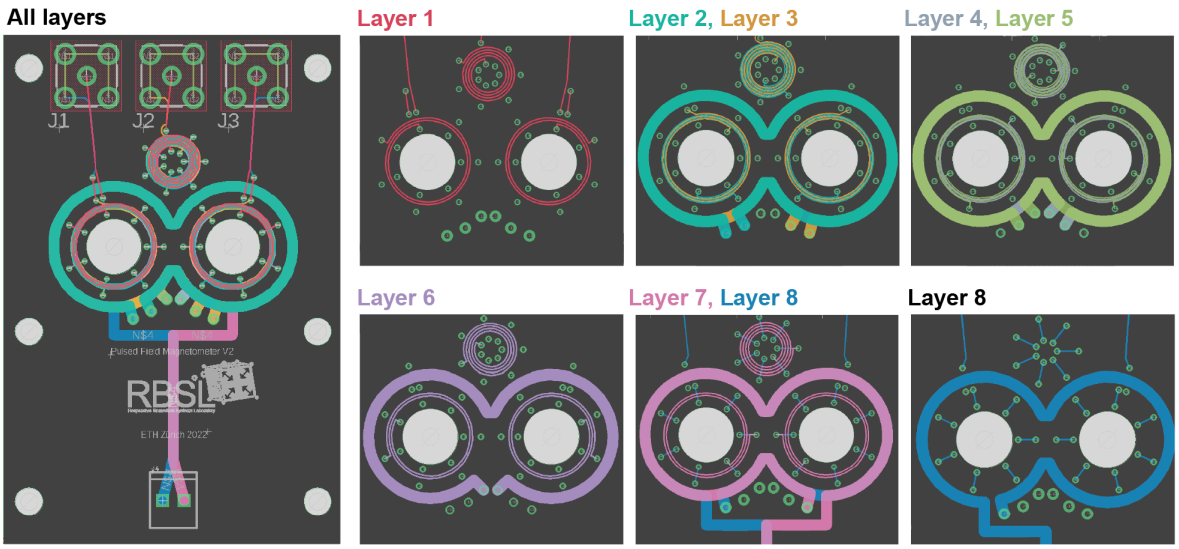

Supplementary Figure S3: Printed circuit board design for sensor board. A detailed view of the geometric layout of the sensor board is provided. Note that, to make the driving field as symmetric as possible, symmetric pairs are formed between several sets of neighboring layers, which are shown together (layers 2-3, layers 4-5, and layers 7-8). These pairs all transmit current in the same rotational sense, but their interconnects between layers are mirrored across the center. To reduce parasitic capacitance of the gradiometer coils, note that within neighboring layers the gradiometer coils are given a rotational offset that reduces direct overlap of the traces. In layer 8, the traces associated with the inductive pickup loops and gradiometer coils serve to connect each layer to another. In total, the pulse coil has 7 turns, the gradiometer coils have 7*(2+⅛)=14.875 turns each, and the field pickup has 7*(4+⅛)=28.875 turns.

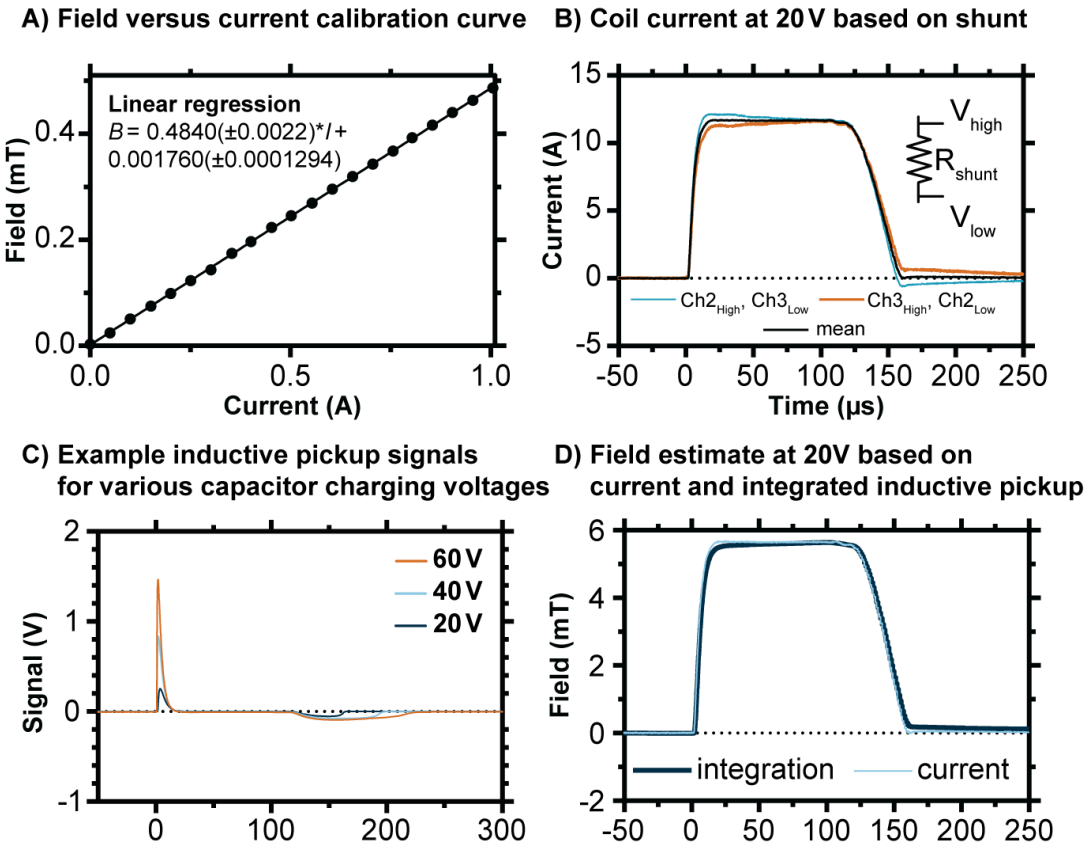

Supplementary Figure S4: Signals from field pickup coil and their conversion to field values. A) A calibration curve was established between DC current measured in the pulse coil (limited to values ≤1A to restrict heating) and the magnetic field experienced in the center of the pulse coil holes, as measured by a 3 axis Hall probe (MetroLab THM1176). In the quasimagnetostatic limit, which is well motivated for the timescales and length scales in question, this relationship between current and field also apply to pulsed fields. Uncertainty values on the fitting parameters reflect their 95% confidence interval. B) The shunt resistor depicted in the pulse circuit shown in Fig S1 (R_{shunt}=0.1015Ω, measured by LCR meter) was used to infer the current delivered to the pulse coil, with the particular case shown here corresponding to a charging voltage of 20V. Note that an artifact appears in the measurements that made it necessary to average between two configurations swapping the high and low probe channels of the shunt. This artifact was later greatly reduced through the incorporation of the inductors on the ground lead of the charging circuit shown in Fig S1A, but is shown here for clarity since this data was used to determine the constant of integration relating the inductive pickup signal to the field. C) Raw voltage signals are shown from the inductive pickup spiral as detected for pulses generated with different capacitor charging voltages (20V, 40V, and 60V, as indicated). Note that Fig 2C of the main text shows these measurements translated into estimates of the field experienced in the loops, found through integration and multiplication by a constant determined through comparison to the shunt current and combined with the calibration curve in panel A. D) Field estimates produced through integration of the inductive pickup signal and measurement of the shunt current are shown for the same 20V pulse depicted in panel B.

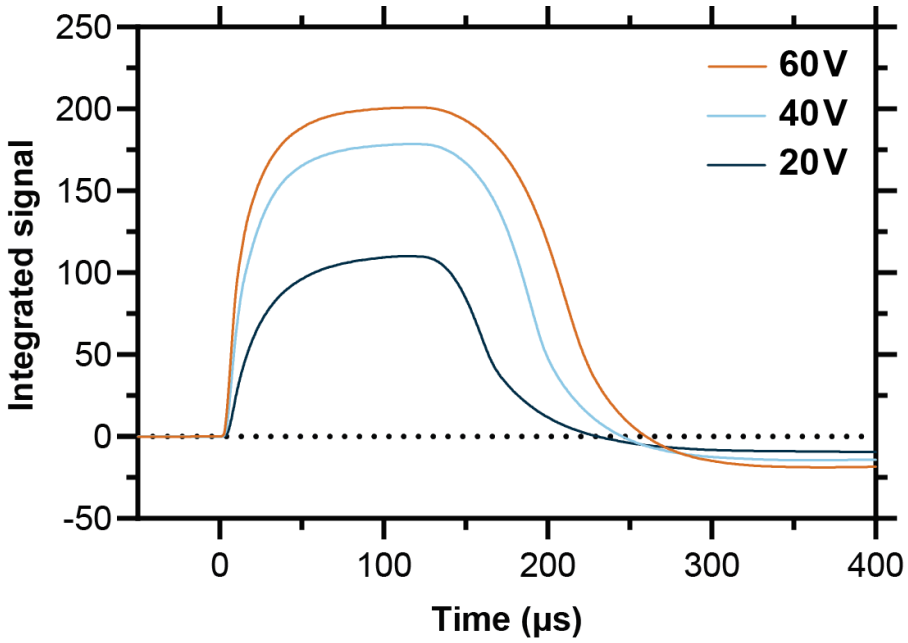

Supplementary Figure S5: Integrated signals of a sample with a concentration of 50 µg/mL Fe and volume of 100 µL with different pulses. The curves are shown with simple integration, such that the result is in arbitrary units that can be expected to be proportional to magnetization of the sample. In general, the constant of integration that converts these signals to magnetization would vary with the detailed geometry of a given sample, including its shape and distance from the sensor. Because these samples had identical geometry, they can be compared directly, and thus it shows a decreasing marginal increase in magnetization with increasing pulse magnitude, an expected result due to saturation of the magnetic nanoparticles. For simplicity and consistency, in the main text, our data has been presented in terms of the measured voltage signals rather than attempting to convert to magnetization curves for each case.

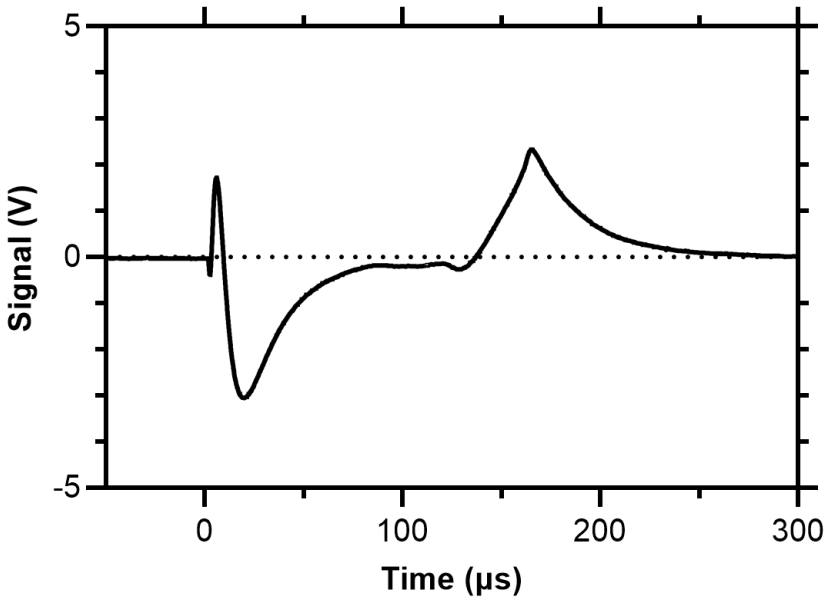

Supplementary Figure S6: Representative background signal of magnetometer output.

For the measurements of dissolved samples of magnetic nanoparticles, background measurements were taken before and after measuring the magnetic nanoparticle sample. The average of the two background measurements was subtracted from the sample measurement to obtain the signal, as shown in Fig. 2E in the main text. The maximum value of the initial peak, corresponding to the sample's magnetization, was interpreted as the main feature of the signal for this sample. To calculate the limit of detection (LOD), we considered the mean and standard error of the four lowest sample measurements, which were at or below the noise floor of our measuring device. The LOD at a 95% confidence interval was calculated as the mean plus 1.645 times the standard error of these samples. The lowest detectable signal obtained by this procedure was 46.7 mV. The relationship between signal and concentration was determined using a linear regression of the four highest concentration samples. From this linear regression, the LOD was found to be 413 ng when expressed in terms of the mass of magnetic material.

The time-resolved measurements of the protease kinetics, as shown in Figs. 4D and 4E in the main text, necessitated a different signal processing pipeline as background measurements could no longer be taken between each data point. The device was let to thermally equilibrate for 1–2 h before any cleavage experiment to minimize thermal drift of the signal. Measurements were started 5 min before addition of the protease to record a background signal. Signals were recovered from the first peak of the raw traces through integration without background correction. Even with extensive thermal equilibration, some residual background drift remained which was corrected for by performing a linear regression on the initial background signals and then correcting for the drift across all signals.

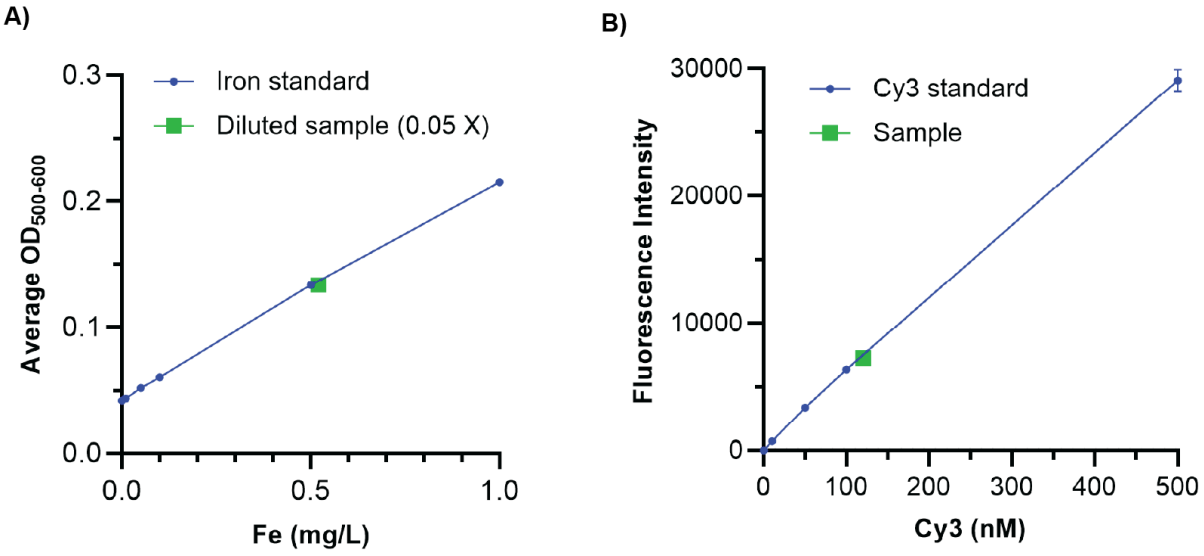

Supplementary Figure S7: Quantification of functional groups on magnetic nanoparticles. Amine-functionalized magnetic nanoparticles were labelled with excess sulfo-Cy3-NHS ester, followed by magnetic separation. The Cy3-labelled particles were resuspended in PBS buffer for analysis. A) Quantification of iron content of the particles. B) Quantification of Cy3 on the particles.

A) Synthesis of DBCO-peptide-NHS

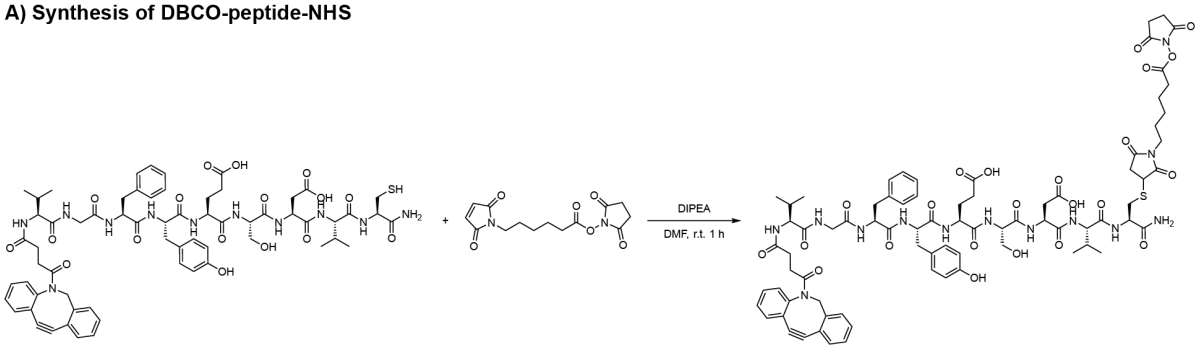

B) HRMS characterization

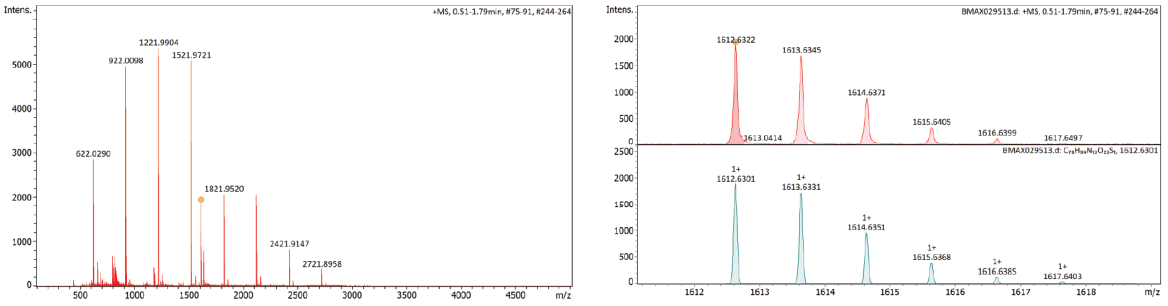

Supplementary Figure S8: Synthesis and characterization of functionalized peptide linker. A) Synthesis of functionalized peptide linker. Peptide was functionalized with NHS ester via a reaction between its terminal cysteine and N-succinimidyl 6-maleimidohexanoate. B) High-resolution mass spectrometry (HRMS) characterization of functionalized peptide.

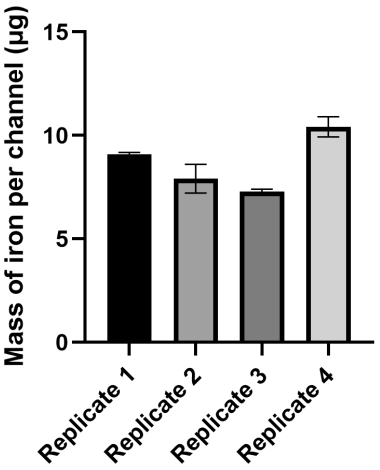

Supplementary Figure S9: Quantification of immobilized MNPs on chip. 6 layers of MNP-peptide-DBCO were sequentially immobilized inside the channel. After being dissolved by HCl, an iron test was performed to quantify the mass of iron for each channel. The graph shows the mean and standard deviation of measurements in triplicates.

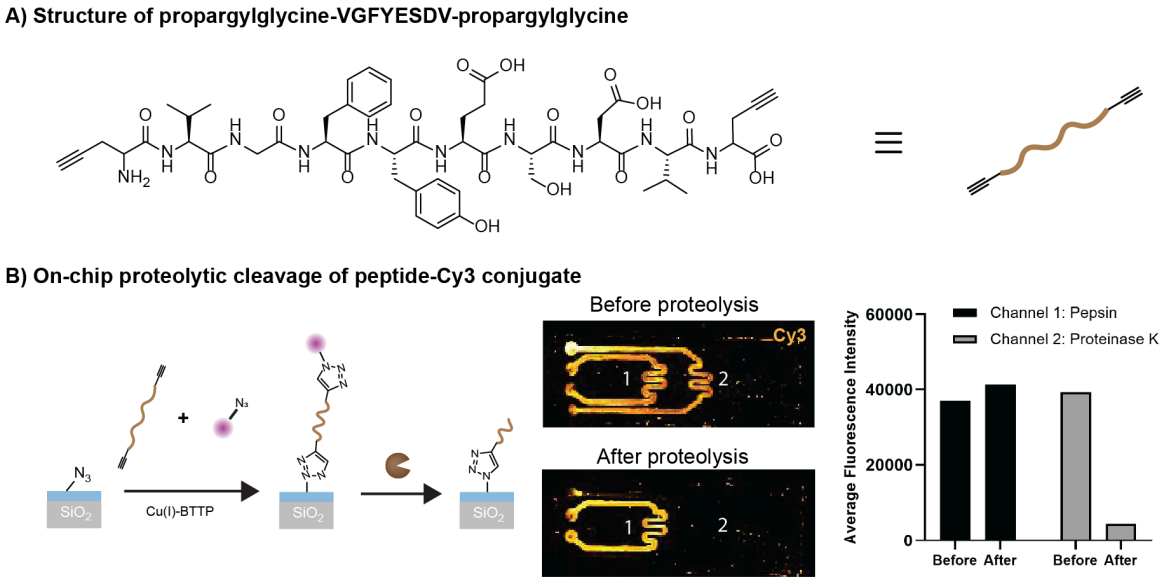

Supplementary Figure S10: Verifying on-chip proteolytic cleavages. A) Structure of bis-alkyne functionalized peptide: propargylglycine-VGFYESDV-propargylglycine. B) Immobilization and proteolytic cleavages of peptide-Cy3 conjugate on chip. The bis-alkyne functionalized peptide and sulfo-Cy3-azide were immobilized on azide-functionalized chip surface via a copper-catalyzed click reaction. Two channels of the chip were then exposed to 0.1 mg/mL pepsin and proteinase K, respectively. Fluorescence image of the chip was captured before and after proteolytic cleavage.

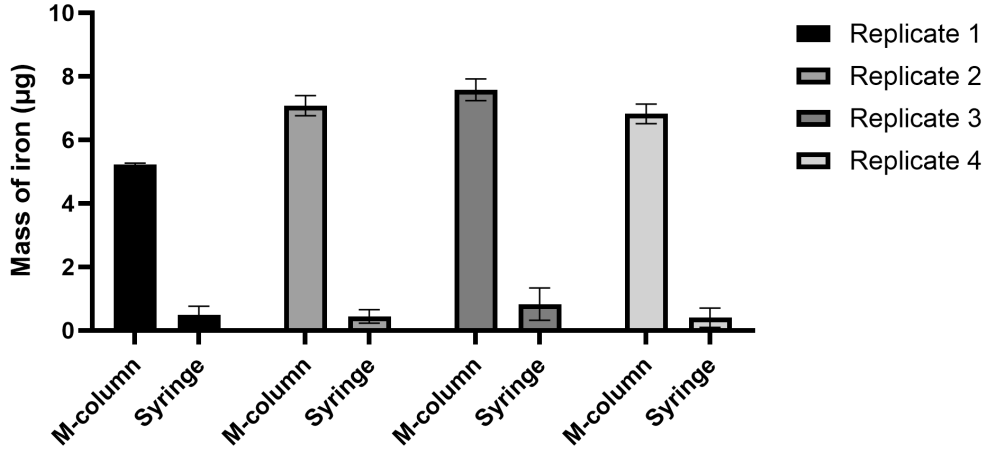

Supplementary Figure S11: Magnetic capture of released MNPs after proteolytic cleavages. After proteolytic cleavages, MNPs in M-column (captured) and in syringe (not captured) were collected, followed by quantification via an iron test. The graph shows the mean and standard deviation of measurements in triplicates.

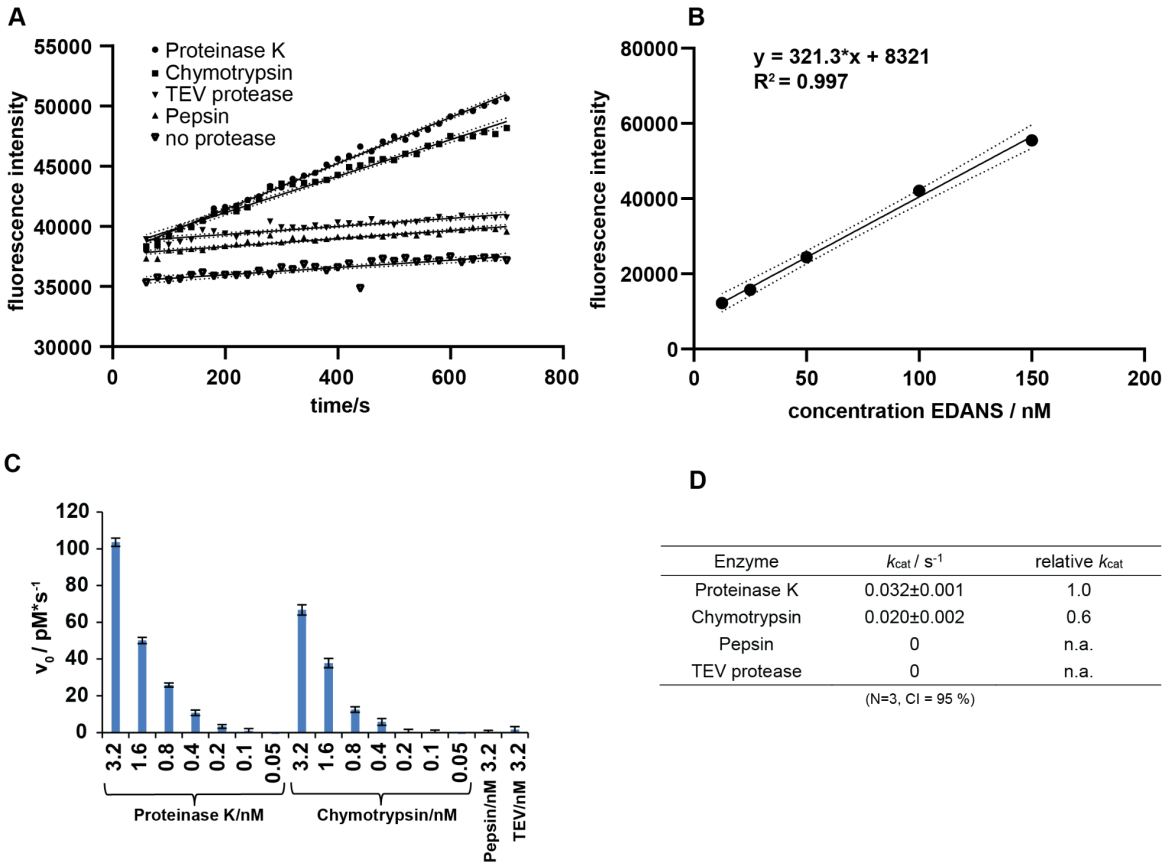

Enzyme	k_{cat} / s^{-1}	relative k_{cat}
Proteinase K	0.032±0.001	1.0
Chymotrypsin	0.020±0.002	0.6
Pepsin	0	n.a.
TEV protease	0	n.a.

(N=3, CI = 95 %)

Supplementary Figure S12: Cleavage efficiency of the peptide VGFYESDV with different proteases. A) Example for the incubation of Dabcyl-VGFYESDVE(EDANS)-NH_2 with 1.6 nM protease. The initial velocity (v_0) was determined from the slope of a linear regression fit minus the slope of the no protease reaction. B) Cleavage product was calibrated towards free EDANS. C) Initial velocities at different protease concentrations (error bar shows the regression slope error with a confidence interval of 95%). The linear behavior of v_0 vs. protease concentration $[E]_0$ indicates maximum velocity ($v_0=v_{max}$). Therefore the catalytic constant k_{cat} was calculated as $v_0/[E]_0$. D) Catalytic constant of the proteases towards Dabcyl-VGFYESDVE(EDANS)-NH_2.

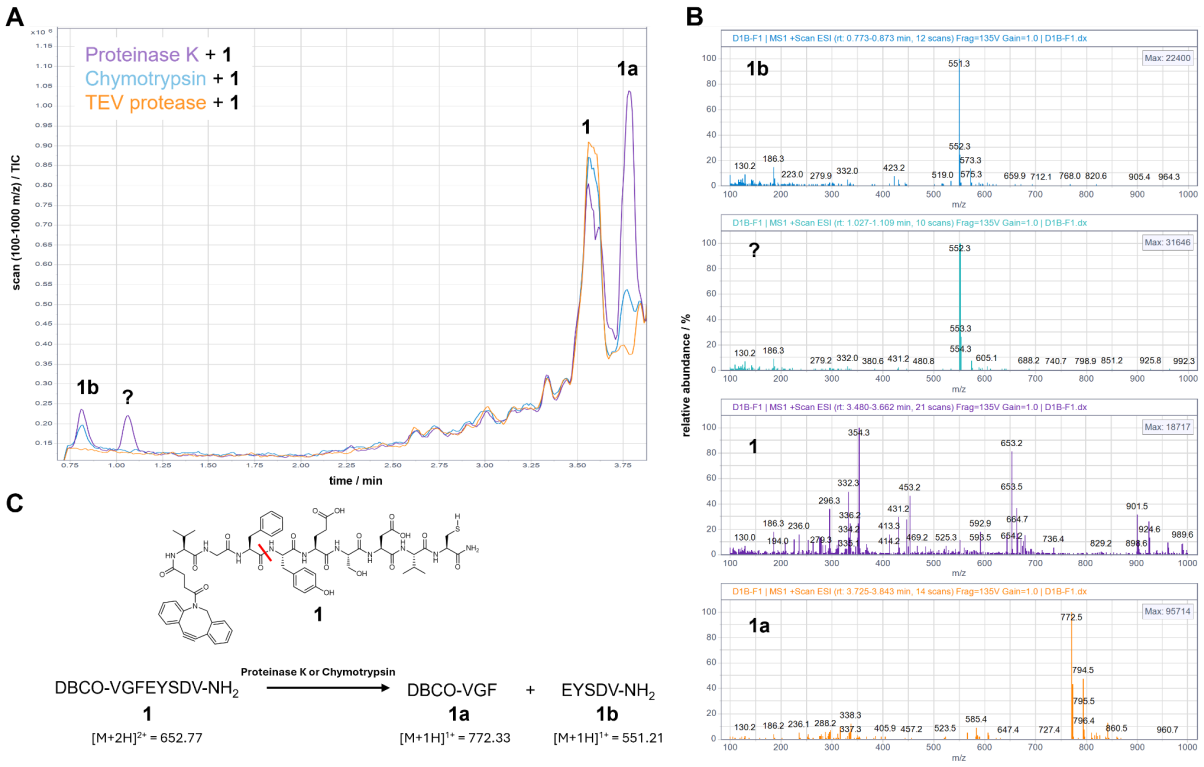

Supplementary Figure S13: Cleavage site determination of the peptide VGFYESDV. A) LC-MS chromatogram showing cleavage products for the reaction with proteinase K and chymotrypsin. B) Corresponding mass spectrum of the novel peaks indicating cleavage C) at the amide bond (red line) of phenylalanine.

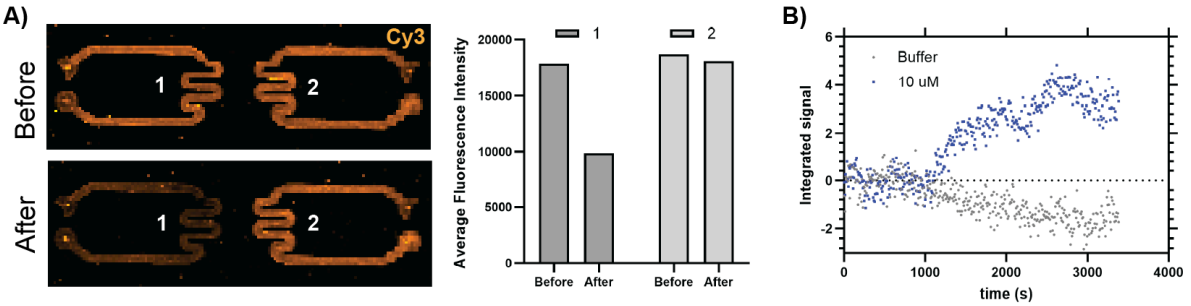

Supplementary Figure S14: On-chip proteolytic cleavage in a buffer containing 10% FBS. A fluidic chip was loaded with Cy3 labeled MNPs by layering between azide-functionalized MNPs and DBCO-peptide functionalized MNPs. Two channels of the chip were exposed to 10 μM chymotrypsin (channel 1) and buffer (channel 2), respectively. (Buffer: 30 mM Tris HCl, 5 mM $CaCl_2$, 10% FBS, pH 8.0) A) Fluorescence scanning of the chip before and after proteolytic cleavage. B) Inductive signal over time for chymotrypsin and buffer. Calculated rates of change in integrated inductive signal are 0.018, and -0.007 V for 10 μM chymotrypsin and buffer, respectively.

Supplementary Tables

Supplementary Table S1: Cost analysis of fluidic chip at laboratory scale.

Item	Quantity needed	Price per unit ($)	Total cost per chip ($)
Microscope glass slide	1 pc	~$27/200 pcs	0.01
PDMS	5 g	~$330/kg	1.65
PDMS-PEG BCP	25 mg	~$260/kg	0.01
MNPs	~10 ug	~ $849/25 mg	0.34
peptide	~8 ug	~ $1000/10 mg	0.80
Total estimated cost ($)			**2.80**

It is worth noting that the cost of chemically modifying fluidic chips is negligible, as multiple chips can be functionalized in parallel, and the chemical reagents used in this study—such as monomers, catalysts, and solvents—are inexpensive. The cost estimation provided for the fluidic chip is based on a laboratory scale. At larger scales, many cost factors can be significantly reduced, including the use of more affordable microfluidic materials instead of lab-grade PDMS, customized synthesis of MNPs rather than commercial MNPs, and reduced costs for large-scale peptide synthesis.

Supplementary Table S2: Cost analysis of sensing device at large scale (estimate).

Item	Quantity needed per device	Price per unit (for >10000) ($)	Total cost per device ($)
MOSFET for pulse circuit	1	0.86	0.86
Variable resistors for balancing	3	0.90	2.71
Variable capacitors	2	5	10
ADA4625-2ARDZ (amplifier, two channel)	1	7.41	7.41
ADP5070AREZ (switching regulator)	1	3.88	3.88
ADP7182AUJZ (negative linear regulator)	1	2.37	2.37
ADP7142ARDZ (positive linear regulator)	1	1.73	1.73
Discharge capacitors (with cost optimization for 20V operation)	3	0.90	2.71
ADSP-BF700KCPZ (digital signal processor chip)	1	6.20	6.20
ADAQ7988BCCZ (analog to digital converter)	1	9.44	9.44
Additional passive components (filter inductors, resistors, capacitors)	N/A	10	10
AC to DC wall adaptor	1	5	5
8 layer printed circuit board	1	10	10
Connectors	N/A	10	10
Structure	1	10	10
Total estimated cost ($)			**92.63**

This rough cost estimate is based on a hypothetical version of the system fully integrated onto a single printed circuit board that incorporates a low noise DC supply for the amplifiers, pulse generation, signal amplification, analog to digital conversion of the signals, and communication with a computer. (In the laboratory prototype version used for data collection, separate printed circuit boards were developed for the pulse circuit, magnetometer coils, and amplification circuit. Data was collected by an oscilloscope and power for the amplifiers was supplied by a filtered AC to DC converter.) The prices for components are estimated based on their extended price for more than 10000 units to take into account economy of scale.

Supplementary Text 1: MATLAB script for controlling oscilloscope

```
% Code to automatically save measurements from Oscilloscope
% authors: Anna Scheeder, Leif Sieben and Michael Christiansen.
% date: 10.06.2024

%% Channel Definitions
% CHANNEL1 = trigger pulse
% CHANNEL2 = field probe
% CHANNEL4 = Amplified signal Magnetometer

%% Connect to Oscilloscope
clear all; close all; clc;
Oscilloscope = visa('agilent', 'USB0::0x0957::0x179A::MY58102499::0::INSTR');
Oscilloscope.InputBufferSize = 8388608;
Oscilloscope.ByteOrder = 'littleEndian';
fopen(Oscilloscope);
fprintf("connected\n");

%% Global Variables
% Set the directory to save folders
dir = 'C:\\Users\\localadmin\\Desktop\\Fan\\OscilloscopeControl\\240717_protease_cleavage';

% Set how many measurements should be recorded
number_of_measurements = 320;

%% Setting up File Directories
fprintf('I will save %d files \n', number_of_measurements);

% Format the directory names
dirName = [dir '\\' datestr(now, 'dd-mm-yyyy HH-MM-SS')];
if exist(dirName, 'dir') == 0
    mkdir(dirName)
end

subdirName = fullfile(dirName);
if exist(subdirName, 'dir') == 0
    mkdir(subdirName)
end

%% Export SignalMagnetometer
% Get time increment and offset for time as x-axis
xInc = str2double(query(Oscilloscope, ':WAV:XINC?'));
xOri = str2double(query(Oscilloscope, ':WAV:XOR?'));

% Pre-allocate arrays
elapsedTime = zeros(1, number_of_measurements);

tic;
for i = 1:number_of_measurements
    elapsedTime(i) = toc;

        % Save as .mat object
    signalMagnetometer = getWaveformData(Oscilloscope, "CHANNEL4", xOri, xInc);
        filename = sprintf('SignalMagnetometer_%d.mat', i);
    save(fullfile(subdirName, filename), 'signalMagnetometer');

        % Save as .csv file
        T = array2table(signalMagnetometer);
        filename = sprintf('SignalMagnetometer_%d.csv', i);
    writetable(T, fullfile(subdirName, filename));

        % Plot during acquisition to monitor
    plot(signalMagnetometer(:, 2), signalMagnetometer(:, 1))
        hold on

        % Save timing info
    filenameTiming = fullfile(subdirName, "Timing.csv");
    writetable(array2table(elapsedTime), filenameTiming)

        fprintf('Saved file %d\n', i)
end

%% Close Connection to Oscilloscope
fclose(Oscilloscope);
delete(Oscilloscope);
fprintf('You are good to go. Have a nice day! \n');
fprintf("disconnected\n");
```

```
%% Function Definitions
function Signal = getWaveformData(Oscilloscope, channel, xOri, xInc)
        % Function to retrieve waveform data from the oscilloscope
        %
        % Inputs:
        %   Oscilloscope - The oscilloscope object
        %   channel - The channel from which to retrieve waveform data (e.g., 'CHANNEL4')
        %   xOri - The origin of the x-axis (time axis)
        %   xInc - The increment value for the x-axis (time axis)
        %
        % Output:
        %   Signal - A matrix where the first column contains the signal amplitudes and the
        %               second column contains the corresponding time values

    fprintf(Oscilloscope, ':WAVeform:FORMat ASCii');
    fprintf(Oscilloscope, sprintf('WAVeform:SOURce %s', channel));

        C = query(Oscilloscope, ':WAVeform:DATA?');
        data = strsplit(C, ',');

        % Pre-allocate arrays
        signalAmpl = zeros(1, length(data));
        signalTime = zeros(1, length(data));

        for i = 1:length(data)
        % Convert strings to numbers
         signalAmpl(i) = str2double(data{1, i});
        % Calculate time of measurement points
         signalTime(i) = xOri + (xInc * (i - 1));
        end

        Signal(:, 1) = signalAmpl;
        Signal(:, 2) = signalTime;
end
```